

RESEARCH

Open Access



IGF1 receptor-targeted black TiO₂ nanoprobe for MRI-guided synergetic photothermal-chemotherapy in drug resistant pancreatic tumor

Kaiwei Xu^{1†}, Lufei Jin^{1†}, Liu Xu^{1†}, Yuchao Zhu¹, Lu Hong¹, Chunshu Pan², Yanying Li^{2,3}, Junlie Yao^{2,3}, Ruifen Zou^{2,3}, Weiwei Tang¹, Jianhua Wang^{1*}, Aiguo Wu^{2,3*} and Wenzhi Ren^{2,3,4*}

Abstract

Pancreatic ductal adenocarcinoma (PDAC) is among the deadliest malignant tumors with features of matrix barrier caused poor drug permeability, and susceptibility to drug resistance. Herein, a PDAC and its stromal cell dual-targeted photothermal-chemotherapy strategy is explored to loosen the matrix and reverse drug resistance. To achieve this goal, black TiO₂-Gd nanocomposites were conjugated with insulin like growth factor 1 (IGF1), and loaded with gemcitabine (GEM) to construct bTiO₂-Gd-IGF1-GEM nanoprobe. In vitro results show that under 808 nm near-infrared irradiation, killing effect of the nanoprobe on drug-resistant MIA PaCa-2 cell is 3.3 times than that of GEM alone. In vivo experiments indicate the synergetic photothermal-chemotherapy not only loosens fibrous matrix of pancreatic tumor model, but also dramatically inhibits tumor growth, and almost completely eradicates the tumor after 12 days of treatment. In addition, relaxation rate of the nanoprobe is 8.2 times than commercial contrast agent Magnevist, therefore boosts the signal of magnetic resonance imaging in pancreatic tumor. In conclusion, our results reinforce that the prepared nanoprobe is promising to break matrix barrier and overcome drug resistance in PDAC.

Keywords: Pancreatic tumor, Drug resistance, Targeted photothermal therapy, Black TiO₂ nanoparticles

Introduction

Pancreatic ductal adenocarcinoma (PDAC) is a severely malignant tumor, with a poor 5-year survival rate of only 9%, and it is estimated to be the second largest contributor to cancer-related death after lung cancer by 2030 [1–3]. Chemotherapy, as a major treatment method for advanced PDAC patients, is commonly unsatisfactory for PDAC, and the effective rate of first line drug gemcitabine (GEM) is less than 20% [4, 5]. There are many causes for chemotherapy failure in PDAC, and two factors are primary. First, PDAC is coated by a “scar”-like matrix barrier, which consists of pancreatic stellate cells, fibroblasts, infiltrating inflammatory cells, and collagen fibers. This dense anatomic structure increases intratumor pressure and decreases blood supply in PDAC, consequently

[†]Kaiwei Xu, Lufei Jin and Liu Xu contributed equally to this work

*Correspondence: wangjianhua@nbu.edu.cn; aiguo@nimte.ac.cn; renwzh@nimte.ac.cn

¹ Department of Radiology, the Affiliated Hospital of Medical School, Ningbo University, 247 Renmin Road, Jiangbei District, Ningbo 315020, Zhejiang, China

² Cixi Institute of Biomedical Engineering, International Cooperation Base of Biomedical Materials Technology and Application, Chinese Academy of Science (CAS) Key Laboratory of Magnetic Materials and Devices & Zhejiang Engineering Research Center for Biomedical Materials, Ningbo Institute of Materials Technology and Engineering, CAS, 1219 ZhongGuan West Road, Ningbo 315201, China

Full list of author information is available at the end of the article



weakens drug delivery capability into tumor. Second, PDAC cell is usually susceptible to drug resistance [6–8]. Therefore, how to break the matrix barrier, improve drug delivery, and reverse drug resistance are main challenges in current stage of PDAC chemotherapy.

In recent years, with the rapid development of nanotechnology, various nanoprobe with unique properties have provided new opportunities for tumor diagnosis and treatment [9–15]. To break through the dense fibrous stroma of pancreatic cancer, plenty of studies have been explored with different strategies, such as depleting the glycans in matrix membrane, reducing the production of stromal cells via inhibition of signal pathway, and fibrous matrix loosen through photothermal nanoprobe [16–18]. When it comes to drug resistance, there are complex mechanisms related, such as aberrant gene expression, deregulated signal pathways, and regulated rate-limiting enzymes, while nanoprobe also exhibit promising in drug-resistance overcoming [19–21]. Photothermal nanoprobe as drug carriers, such as gold nanoshells, gold nanorods, WO_3 and WS_2 , have been reported to destroy the dense matrix barrier of pancreatic cancer and enhance the chemosensitivity of drug-resistant cells, and therefore can eradicate drug-resistant PDAC cells [22–26]. These studies prove nanoprobe exert a great killing effect on PDAC when combined with photothermal-chemotherapy synergistic therapy, which is a promising tumor treatment method.

Given all of that, nanoprobe-based photothermal-chemotherapy strategy has emerged potential application in treatment of PDAC through hyperthermal induced matrix loosening, drug penetration improving, as well as drug resistance overcoming. Although targeting molecule-modified nanoprobe have been convinced to raise drugs accumulation in tumor. However, most of actively targeted nanoprobe are only designed to bind with PDAC cells, while are lack of targeting on both of cancer cells and stromal cells which probable more conducive for drug penetration and accumulation in PDAC. It is obviously that select an optimum binding site is the primary factor for dual targeted drug delivery. Insulin like growth factor 1 receptor (IGF1R) is ubiquitously expressed in 40–90% of PDAC cells and stromal cells, but is lowly expressed in normal pancreas. More excitingly, the expression of IGF1R is further elevated in drug-resistant PDAC cells [6, 27]. Meanwhile, studies have found that IGF1R plays critical functions in occurrence, development, invasion and metastasis of PDAC mainly through K-Ras or MAPK mediated signal pathways. Therefore, IGF1R is an ideal binding site for design of dual targeted drug delivery system.

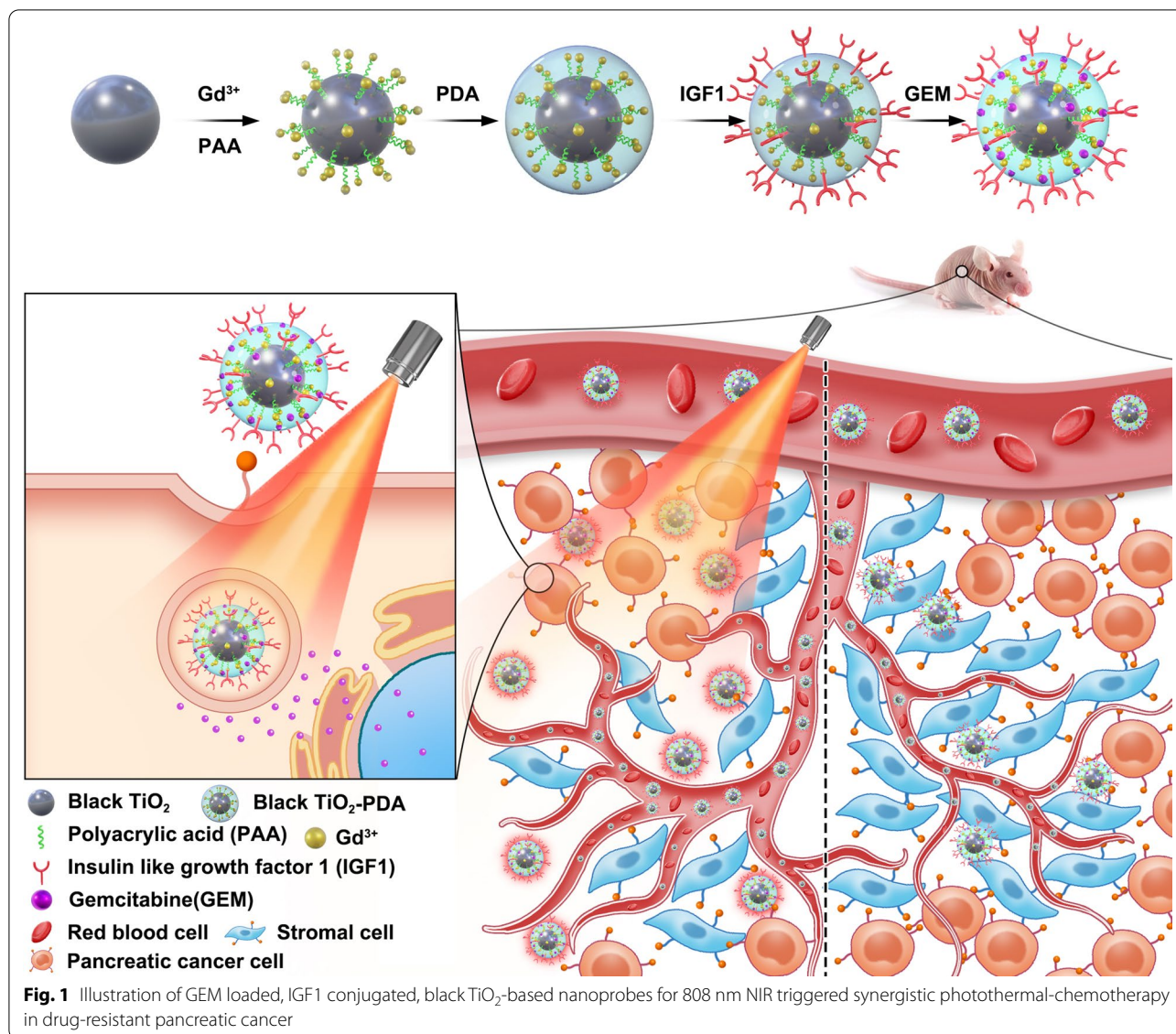
Besides target molecule, photothermal agent is another essential factor in photothermal-chemotherapy strategy.

Black TiO_2 (b TiO_2) nanoparticles, with the advantages of elevated photothermal conversion efficiency, stable structure, and low toxicity, have been initially applied in photothermal therapy by our group [28]. Soon afterwards, b TiO_2 nanoparticles were widely explored in cancer treatments, such as doxorubicin carriers in photothermal-chemotherapy of breast cancer, modified with CD133 antibody and DOTA-Gd for MRI-guided photothermal therapy of pancreatic cancer stem cells, as well as other reported b TiO_2 -based photothermal-photodynamic therapy, photothermal-sonodynamic therapy and so on [29–33]. All these findings prove b TiO_2 are promising nanoprobe in photothermal-chemotherapy of cancer. Herein, to break the matrix barrier and reverse drug resistance, b TiO_2 nanoparticles were coupled with gadolinium acetate, IGF1 polypeptide, and GEM to construct b TiO_2 -Gd-IGF1-GEM nanoprobe. As shown in Fig. 1, the b TiO_2 -Gd-IGF1-GEM nanoprobe are designed to specially bind with both of PDAC cells and stromal cells, subsequently loosen the matrix barrier, enhance drug permeability and reverse drug-resistance under NIR triggered photothermal effect. In vivo results show that after 12 days of treatment, average tumor size is $0.3 \pm 0.4 \text{ mm}^3$ in photothermal-chemotherapy group, while the size is $609.0 \pm 153.7 \text{ mm}^3$ in control group, which well clarifies the promising application prospect of above proposed nanoprobe in PDAC.

Materials and methods

Reagents

Dopamine hydrochloride, sodium borohydride (NaBH_4), TiO_2 nanoparticles, polyacrylic acid MW2000 (PAA MW2000), tris (hydroxymethyl) aminomethane acetate salt ($\text{C}_4\text{H}_{11}\text{NO}_3 \cdot \text{C}_2\text{H}_4\text{O}_2$), 3-(4,5-di-methylthiazol-2-yl)-2,5-diphenyltetrazolium bromide (MTT), dimethyl sulfoxide (DMSO) were acquired from Aladdin Industrial Inc (Shanghai, China). 1-Ethyl-3-[3-dimethylaminopropyl] carbodiimide hydrochloride (EDC), Gadolinium nitrate hexahydrate ($\text{GdN}_3\text{O}_9 \cdot 6\text{H}_2\text{O}$), *N*-hydroxysuccinimide (NHS), Rhodamine 123 ($\text{C}_{21}\text{H}_{17}\text{C}_1\text{N}_2\text{O}_3$) were obtained from Macklin Biochemical Co., Ltd (Shanghai, China). Carboxyl polyethylene glycol amino group (NH_2 -PEG-COOH) were obtained from Yare Bio Co., Ltd (Shanghai, China). Recombinant human IGF1 protein (ab270062) was purchased from Abcam Bio Co., Ltd (England). Gemcitabine ($\text{C}_9\text{H}_{11}\text{F}_2\text{N}_3\text{O}_4$) was purchased from MedChemExpress Co., Ltd (USA). DMEM medium, 0.25% Trypsin–EDTA was acquired from Gibco (Grand Island, USA). Penicillin–streptomycin liquid, phosphate buffer saline (PBS) came from GE Healthcare HyClone (LA, USA). 4% formaldehyde solution, Phalloidin, Fluorescein Isothiocyanate Labeled (FITC), Hoechst 33258 ($\text{C}_{25}\text{H}_{24}\text{N}_6\text{O} \cdot 3\text{HCl}$), RIPA buffer were obtained



from Solarbio Biotech Co., Ltd (Beijing, China). The calcein-AM/PI double stain kit came from Yeasen Biotechnology Co., Ltd (Shanghai, China). Protease inhibitor Cocktail was purchased from Bimake Biotechnology Co., Ltd (USA). ECL chromogenic solution was purchased from Adavanta Co., Ltd (USA). PVDF membrane was purchased from Millipore Co., Ltd (USA). Skim milk powder was purchased from Yili Co., Ltd (Inner Mongolia, China). Pre-stained protein MARKER (BIO-RAD) was purchased from Thermo Fisher Scientific Inc (USA). BCA Protein Assay Kit was obtained from Beyotime Biotech Co., Ltd (Shanghai, China). β -Actin Mouse Monoclonal Antibody was purchased from Santa Cruz Biotech Co., Ltd (USA). Anti-IGF1R antibody was acquired from Bioss Biotech Co., Ltd (Beijing, China).

Preparation of bTiO₂ nanoparticles

Using NaBH₄ as the reducing agent, the TiO₂ was reduced to bTiO₂. First, 1 g of TiO₂ powders were combined with NaBH₄ at a mass ratio of 1:1 for 30 min, then were put inside a tube furnace with a heating rate of 10 °C/min. The temperature was increased to 350 °C in an argon atmosphere, and the reaction lasts for 3 h. The prepared bTiO₂ nanoparticles were rinsed with ultrapure water and were centrifuged thrice minimum to remove NaBH₄. Finally, the bTiO₂ nanoparticles were dried for later using.

Synthesis of bTiO₂-Gd-COOH

Gadolinium acetate tetrahydrate, dopamine hydrochloride and NH₂-PEG-COOH were employed for the

modification of the bTiO₂ nanoparticles. 100 mg of bTiO₂ powders were dissolved into ultrapure water (100 mL) and were dispersed via ultrasound. Then ultrapure water was introduced to the bTiO₂ solution to 90 mL. 500 mg of PAA2000 powders were dissolved into 10 mL of ultrapure water and were stirred magnetically. Next, the bTiO₂ mixture was combined with PAA2000 and stirred for 5 h at room temperature (RT). The dispersions were next collected and centrifuged at 12,000 rpm for thrice. The bTiO₂-PAA nanoparticles were dissolved in 90 mL of ultrapure water. 10 mL of Gadolinium Acetate Tetrahydrate (1 mg mL⁻¹) were added in bTiO₂-PAA dispersions. After stirring for 3 h, the dispersions were collected and centrifuged at 12 000 rpm thrice, then obtained bTiO₂-Gd were dispersed in 10 mL of ultrapure water. The bTiO₂-Gd dispersions were added in 80 mL of 10 mM Tris (PH8.5). After ultrasound for 10 min, the 2 mL of dopamine hydrochloride (75 mg mL⁻¹) was introduced dropwise into this reaction system and stirring at RT for 1 h. The bTiO₂-Gd-PDA dispersions were collected by centrifugation. Subsequently, the dispersions were dispersed into 50 mL of ultrapure water. After ultrasound for 10 min, NH₂-PEG-COOH solutions were added dropwise to the bTiO₂-Gd-PDA and stirring for 24 h. Finally, the bTiO₂-Gd-COOH dispersions were centrifuged at 12,000 rpm, prior to storage in 10 mL of ultrapure water.

Conjugation of IGF1 Peptide

bTiO₂-Gd-COOH nanoparticles were conjugated with IGF1 peptide by EDC/NHS activated amide bonds. Briefly, 5 mL of bTiO₂-Gd-COOH dispersions were resuspended in 45 mL of ultrapure water. 15 mg EDC and 20 mg NHS were dissolved in the dispersions, followed by stirring at RT for 20 min. Subsequently, 100 µL of IGF1 peptide (1 µg µL⁻¹) were added and stirred for 12 h. The prepared bTiO₂-Gd-IGF1 was collected by centrifugation and stored at 4 degrees.

Preparation of bTiO₂-Gd-GEM and bTiO₂-Gd-IGF1-GEM

2 mL of GEM (4 mg mL⁻¹) were introduced to 8 mL of bTiO₂-Gd-COOH (0.75 mg mL⁻¹) and bTiO₂-Gd-IGF1 (0.75 mg mL⁻¹) respectively, followed by stirring for 24 h. GEM loaded nanocarriers (bTiO₂-Gd-GEM or bTiO₂-Gd-IGF1-GEM), the nanoparticles were centrifuged, followed by storage in ultrapure water. The GEM loading efficiency was computed based on the drug's UV-visible absorption, as we reported earlier [34, 35]. In short, following centrifugation, supernatants with GEM were obtained. Next, we assessed the accumulated and free GEM (0–100 µg mL⁻¹) UV-visible absorptions, as well as the GEM concentration-absorption curve. Lastly, the GEM loading amount on

the nanocarriers was computed as follows: loading efficiency = ((total GEM – GEM in supernatant) ÷ nanocarrier amount) × 100%.

Characterization

The nanoprobe microstructure was evaluated via transmission electron microscopy (FEI Tecnai F20). The nanoprobe zeta potential and nanoprobe size distribution were next examined via a particle-size zeta potential analyzer (Nano ZS, Malvern Instruments Ltd, England), and by implementing a UV-visible spectrophotometer (T10CS, Persee General Equipment Co., Ltd, China), UV-visible absorption spectra were assessed. Infrared (IR) spectra of the nanoprobe were obtained from a Fourier transform infrared spectrometer (FTIR, Thermo Nicolet 6700, US). The nanoprobe element content was measured via induction coupled plasma optical emission spectrometry (ICP-OES, Spectro Analytical Instruments GmbH, Germany). Further, by employing a MR scanner system utilizing a magnetic field of 1.5 T, MR imaging and relaxivity capabilities were tested. The nanoprobe photothermal stability and effectiveness were assessed via an infrared (IR) thermal imaging apparatus (Optris Infrared Thermometers, Germany) and 808 nm semiconductor laser (BWT Beijing LTD, China).

Assessment of photothermal efficiency and photostability

To test photothermal properties, bTiO₂-Gd-COOH nanoparticles with different Ti concentrations were added to cuvette and irradiated with various power densities from an 808 nm laser. The values of temperature for bTiO₂-Gd-COOH dispersions were documented every 10 s using an IR thermal imaging apparatus (MAG-V30, Vst Light & Technology Ltd, China), and we simultaneously mapped the images of real-time thermal dispersion. We have summarized the different aforementioned situations below: (1) 1 mL of nanoparticles (150 µg mL⁻¹ of Ti concentration) receiving irradiation with 808 nm laser with different power densities (0.4–2.0 W cm⁻²) for 10 min; (2) Varying nanoparticle concentrations (0–150 µg mL⁻¹ of Ti concentration) were irradiated through an 808 nm laser (1.2 W cm⁻²) for 10 min; (3) For detecting nanoparticle photostability, the bTiO₂-Gd-COOH dispersions (150 µg mL⁻¹ of Ti concentration) were also irradiated with an 808 nm laser (1.2 W cm⁻²) every 5 min for over 6 on/off repeating cycles. The resulting images were collected, and the temperature values fitted in time-temperature curves.

pH-responsive and NIR-triggered drug release

To evaluate drug release, in three dialysis bags, 2 mL bTiO₂-Gd-IGF1-GEM (GEM: 3 µg mL⁻¹) was placed, and each dialysis bag was immersed in 20 mL PBS buffer

solution with pH of 7.4, 5.0 and 5.0 respectively. 1 mL of dialysate was withdrawn and the same quantity of PBS buffer was introduced to keep the same quantity of buffer equal at 1 h, 2 h, 3 h, 4 h, 5 h, 8 h, 12 h, 24 h, and 27 h, respectively. Upon collection of the solution, the solution with pH 5.0 received irradiation with a 1.2 W cm^{-2} near-infrared laser for 15 min. The drug release was monitored via UV-Vis spectrophotometer, and the drug release was computed based on the drug release dose absorption curve.

In vitro MRI

The MRI and MR relaxivity of nanoprobe were evaluated by 1.5 T MRI scanner apparatus. The nanoprobe with varying Gd concentrations (0.025 mM, 0.05 mM, 0.1 mM, 0.2 mM, 0.4 mM) were placed in a tube to measure the relaxation rate. At the same time, the commercial contrast agent Magnevist was adjusted to the control Gd concentration. We obtained the specific longitudinal and transverse, namely (r_1) and (r_2) relaxivities from the rate of relaxation R_1 ($1/T_1$) and R_2 ($1/T_2$) slopes accordingly. The T_1 -weighted MRI characteristics of nanoparticles at varying concentrations of Gd were obtained from the same MRI apparatus, and parameters were adjusted as shown below: T_1 spin echo sequence, $TE = 18.20 \text{ ms}$, $TR = 200.00 \text{ ms}$, $FOV = 100 \text{ mm} \times 100 \text{ mm}$, slice width = 2.0 mm, 1.5 T.

Expression of IGF1R in different PDAC cell lines

The IGF1R levels in the hTERT-HPNE pancreatic ductal epithelial cells, BxPC-3 PDAC cells, Panc-2 PDAC cells, and MIA PaCa-2 PDAC cells were quantified via western blot analysis. Firstly, the total proteins of the above four cells were extracted and the protein quantification and concentration were measured. Then, 10% concentration of concentrated gel and separation gel were selected according to the molecular weight of the protein. The solidified PAGE gel was installed on the electrophoresis tank, $1 \times$ electrophoresis buffer between two pieces of glass to join until more than plastic plane, and gently pull out a comb. According to different protein concentrations, protein samples of equal mass were taken and added to each well. Meanwhile, appropriate protein markers were selected and added to the outermost well according to different protein molecular weights. Constant pressure method was used for protein electrophoresis. PVDF membrane of appropriate size was selected for membrane transfer. After membrane transfer, PVDF membrane was carefully clamped out and sealed with protein. The PVDF membrane was clamped out and cleaned repeatedly for 3 times. The PVDF membrane was treated with the configured primary antibody, and the membrane was kept on a horizontal shaker at 4°C

for 6 h. Finally, primary antibody was recovered, PVDF membrane was clipped out and washed 3 times, PVDF membrane was incubated with the configured secondary antibody, and placed on a horizontal shaker at 4°C for 1 h. Upon incubation, PVDF membrane was clipped out and washed 3 times. Then, appropriate ECL chemiluminescence was configured according to the size of the membrane and added to the PVDF membrane. The membrane was exposed in a chemiluminescence imager, and the results were recorded.

Cell culture

The MIA PaCa-2 PDAC, Panc-2 PDAC, BxPC-3 PDAC and hTERT-HPNE human pancreatic ductal epithelial cell lines were acquired from the Cell Bank of the China, Academy of Sciences (Shanghai, China). The MIA PaCa-2, Panc-2, BxPC-3 and hTERT-HPNE cell lines were grown in complete DMEM medium, containing 10% FBS, 100 U mL^{-1} penicillin and 100 U mL^{-1} streptomycin, and incubated at 37°C with 5% CO_2 .

Cytotoxicity of nanoprobe

For cytotoxicity analysis of $\text{bTiO}_2\text{-Gd-COOH}$ and $\text{bTiO}_2\text{-Gd-IGF1}$, MIA PaCa-2 PDAC cells were seeded in 96-well plates (1×10^4 cells per well) and grown for 24 h. Next, different concentrations of nanoprobe ($50\text{--}300 \mu\text{g mL}^{-1}$) were added into each well. Following 20 h, $10 \mu\text{L}$ of MTT reagent (5 mg mL^{-1} in PBS) was introduced to each well and kept for additional 4 h. Finally, the mediums were suctioned off, and formazan crystals were resuspended by DMSO. The absorbances of formazan solutions were detected using a microplate absorbance reader (BioradiMARK™, USA) at 490 nm and 550 nm, and cell viabilities were computed.

Cellular uptake characterization

To measure cell-targeting capability of IGF1 conjugated nanoprobe, X-ray fluorescence microscopy at Shanghai Synchrotron Radiation Facility (SSRF, Shanghai, China) was used. First, cells were seeded on sterile Malay films and placed in a cell incubator for 24 h, then cultured in DMEM and $\text{bTiO}_2\text{-Gd-COOH}$, $\text{bTiO}_2\text{-Gd-IGF1}$, $\text{bTiO}_2\text{-Gd-IGF1-GEM}$ for 2 h, respectively. Next, cells were twice PBS-rinsed before fixation in 4% formaldehyde solution. Finally, elemental fluorescence of Ti and Cl in cells was obtained. The X-ray energy was 10 keV, and the beam spot was $0.5 \times 0.5 \mu\text{m}^2$. Elemental maps of Ti, Cl in cells were acquire.

For statistical analysis of targeting ability, MIA PaCa-2 cells were seeded in 6-well plates for 24 h, and maintained with $\text{bTiO}_2\text{-Gd-COOH}$, $\text{bTiO}_2\text{-Gd-IGF1}$ for another 2 h. Next, the cells were digested by nitric

acid and hydrofluoric acid. The element content in cells were determined via ICP-OES.

For furthermore proving targeting capability, bTiO₂-Gd-COOH and bTiO₂-Gd-IGF1 nanoprobcs were labelled by fluorescence dye rhodamine 123, and were determined by laser confocal microscope at excitation wavelength of 488–505 nm and emission wavelength of 515–575 nm. MIA PaCa-2 cells (1 × 10⁵ cells) were grown on a 35 mm petri dish and placed in an incubator for 24 h, prior to treatment with the same concentration of DMEM, bTiO₂-Gd-COOH, and bTiO₂-Gd-IGF1 for 2 h. Next, the cells were PBS-rinsed before fixation in 4% paraformaldehyde, and treatment with 0.2% Triton X-100. Followed, 1% BSA solution was used for blocking non-specific interacting sites, and the cells were incubated by employing 50 μg mL⁻¹ FITC-Ghost Pencyclic peptide and 2 μg mL⁻¹ Hoechst 33342 for cytoskeleton and nucleus staining.

Photothermal therapy synergistic chemotherapy evaluation

MIA PaCa-2 cells were grown in the plates containing 96 wells (1 × 10⁴ cells per well), followed by incubation in DMEM, GEM, bTiO₂-Gd-COOH, bTiO₂-Gd-GEM, and bTiO₂-Gd-IGF1-GEM or bTiO₂-Gd-IGF1 for 2 h. Ti concentrations of bTiO₂ contained groups were 150 μg mL⁻¹, the GEM concentration of the GEM alone group was consistent with that of the other groups, which was 3 μg mL⁻¹. 2 h later, the old media was suctioned off and fresh DMEM was added, and then each well underwent irradiation with 808 nm NIR laser for 1–4 min at power densities of 1.2 W cm⁻², respectively. MTT was subsequently employed to assess cell viability.

In vivo toxicity evaluation of nanoprobcs

For animal experiments, animal care and handling procedures were in agreement with the guidelines of the Regional Ethics Committee for Animal Experiments at Ningbo University (Permit No. SYXK Zhe 2019-0005). To assess nanoparticle toxicity in vivo, 12 normal Balb/c mice (4–6 weeks old) were arbitrarily separated into 3 groups. The mice received intravenous injection of 150 μL of PBS, bTiO₂-Gd-COOH or bTiO₂-Gd-IGF1. The nanoprobe dosage was 20 mg kg⁻¹. This treatment was carried on for a month, and we documented their weight and behavior. At the end of the month, all mice were euthanized. One mouse from each group was tested for routine blood. Major organs like heart, liver, spleen, lung and kidney were fixed in 10% formalin prior to hematoxylin and eosin (H&E) staining.

In vivo imaging and synergetic photothermal-chemotherapy

Tumor models were developed in male balb/c nude mice (4–6 weeks). MIA PaCa-2 cells (1 × 10⁶ cells for each mouse) in DMEM were subcutaneously injected in the right flank of the animals. The mice were arbitrarily separated into 6 groups (5 mice per group). The tumor size was measured with a digital caliper. Tumor volume = 4/3 × π × (tumor radius)³. Our experiments were initiated once tumors reached 50 mm³. The mice received intratumoral administration of 100 μL of PBS, GEM, bTiO₂-Gd-IGF1, bTiO₂-Gd-IGF1-GEM. The concentration of GEM was 3 μg mL⁻¹ in GEM groups and the concentration of Ti concentration was 150 μg mL⁻¹ in the bTiO₂ groups. Meanwhile, for MR imaging, commercial contrast agent magnevist with a Gd concentration of 3 μg mL⁻¹ was injected. Following 24 h of incubation, mice underwent intraperitoneal injection of 8 wt% of chloral hydrate solution, followed by irradiation, in the presence or absence of 808 nm NIR laser for 5 min at 1.2 W cm⁻². The tumor temperature alterations were documented using an infrared thermometer (PI400, Optris, Germany). From each group, one mouse was arbitrarily chosen and euthanized following the irradiation of NIR, and the tumor injury was analyzed via H&E staining. We monitored tumor sizes for 12 days and computed the volumes based on the aforementioned tumor volume formula. Mice body weights were also documented for 2 weeks.

Statistical analysis

Data are expressed as mean ± standard deviation, and via the Student's t test were compared. P < 0.05 was adjusted as the significance threshold.

Results and discussion

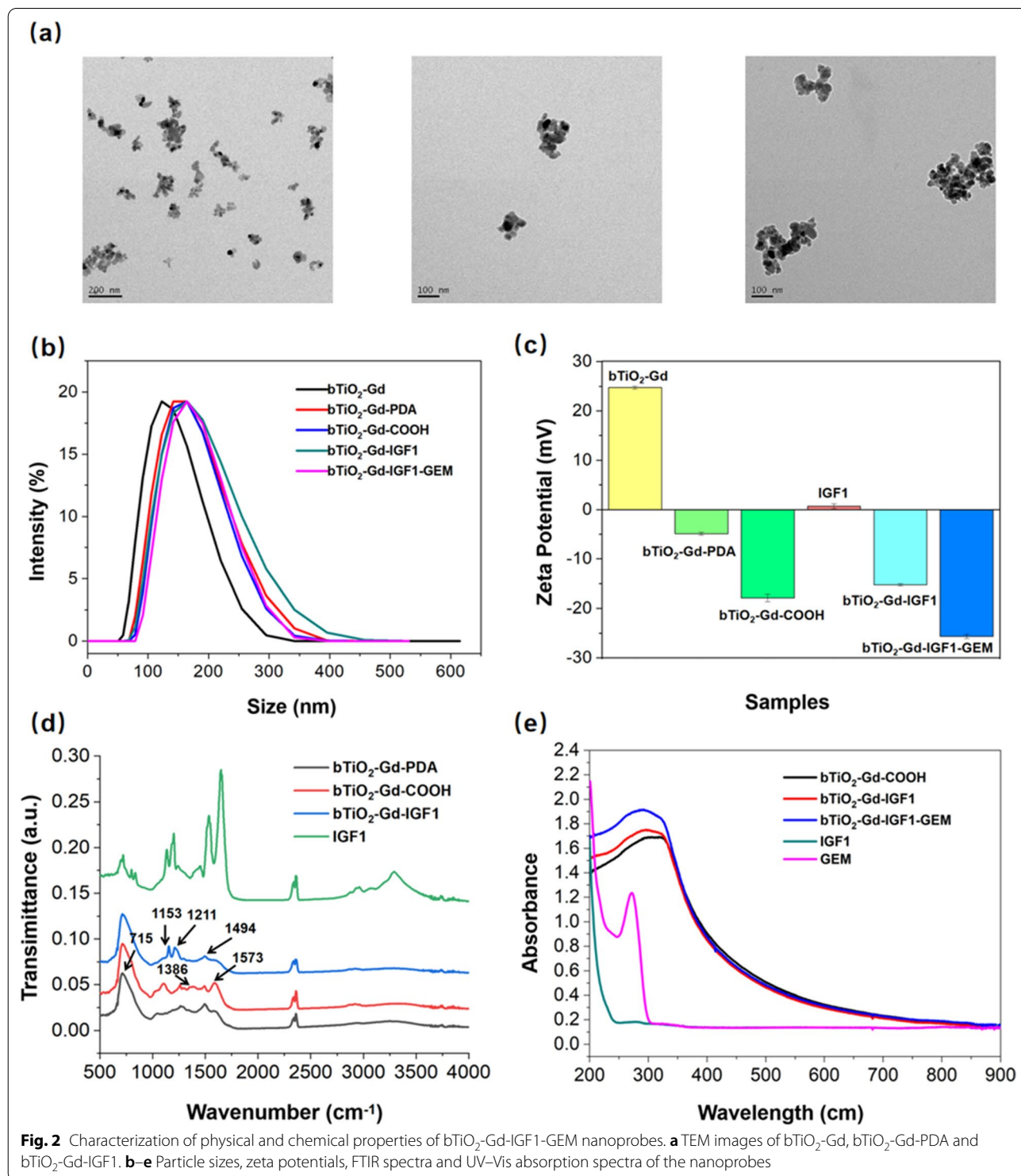
Characterizing the bTiO₂-Gd-IGF1-GEM nanoprobcs

The bTiO₂-Gd-IGF1-GEM synthesis process is showed in Fig. 1. To improve dispersibility of bTiO₂, meanwhile to supply coordination sites for contrast agent Gd, bTiO₂ nanoparticles were coated with PAA through hydrogen bonding and charge adsorption between positive charge of bTiO₂ and carboxyl of PAA. Then the nanoparticles were complexed with Gd³⁺ through coordination bonds to form bTiO₂-Gd nanoprobcs. Polydopamine (PDA), with phenolic hydroxyl polymerized special cyclic structures, can supply binding sites for peptide conjugation and drug loading, and is usually used for surface coating of nanoparticles [36, 37]. To further improve dispersibility of obtained bTiO₂-Gd-PDA, the nanoprobcs were conjugated with amino group of NH₂-PEG-COOH through Michael

addition reaction. The formed bTiO₂-Gd-COOH nanoparticles have good dispersibility. Gemcitabine (GEM), a first-line chemotherapy drug for PDAC, was loaded by bTiO₂-Gd-COOH via pi-pi stacking and/or hydrogen binding [38]. Finally, IGF1 peptides underwent

conjugation on the nanoparticles via EDC/NHS-activated amide bond to form bTiO₂-Gd-IGF1 nanoprobles [21].

As shown in Fig. 2a, TEM images indicate diameters of bTiO₂-Gd, bTiO₂-Gd-PDA and bTiO₂-Gd-IGF1 nanoprobles



are 60 nm, from left to right respectively. The mean hydrated size of bTiO₂-Gd, bTiO₂-Gd-PDA, bTiO₂-Gd-COOH, bTiO₂-Gd-IGF1, bTiO₂-Gd-IGF1-GEM are about 123.3 nm, 153.2 nm, 149.2 nm, 158.8 nm and 159.9 nm, respectively, in Fig. 2b. The data show that with modification of related components, particle sizes of the nanoprobe gradually increase, bTiO₂-Gd-IGF1-GEM of this size has good biocompatibility and is still suitable for tumor treatment. In addition, zeta potentials of bTiO₂-Gd, bTiO₂-Gd-PDA, bTiO₂-Gd-COOH, IGF1 polypeptide, bTiO₂-Gd-IGF1 and bTiO₂-Gd-IGF1-GEM are about 24.73 mV, -4.85 mV, -17.87 mV, 0.67 mV, -15.27 mV and -25.67 mV, respectively. In general, traditional white TiO₂ nanoparticles show negative zeta potential owing to surface hydroxyl groups. Our previous investigation prove bTiO₂ nanoparticles exhibit positive zeta potential which probably due to reduction induced abundant oxygen vacancies on the nanoparticles surface [20]. Besides, coordinated with Gd³⁺ also increase positive charge, so the surface charge of bTiO₂-Gd nanoprobe appear positive charge. After coating with PDA, surface charge of bTiO₂-Gd-PDA nanoprobe are changed to negative. Zeta potential of bTiO₂-Gd-IGF1-GEM reaches -25.67 mV after modification with NH₂-PEG-COOH, IGF1 and GEM, which is more suitable for in vivo delivery when compared with positive surface charge.

Figure 2d is the FTIR spectra of nanoprobe and IGF1 polypeptides. There is a sharp peak near 715 cm⁻¹ in bTiO₂-Gd-PDA, bTiO₂-Gd-COOH, and bTiO₂-Gd-IGF1, which is attributed to characteristic absorption peak of Ti-O [39]. After modified NH₂-PEG-COOH through Michael addition reaction, bTiO₂-Gd-COOH nanoprobe exhibit carboxylic acid symmetrical and asymmetrical stretching vibrations at 1386 cm⁻¹ and 1573 cm⁻¹ [40]. In bTiO₂-Gd-IGF1 nanoprobe, there are characteristic peaks at 1494 cm⁻¹, 1153 cm⁻¹, and 1211 cm⁻¹, which suggests IGF1 polypeptide has been successful connected with bTiO₂-Gd-COOH nanoprobe. UV-visible spectra of various samples are provided in Fig. 2e, relative to bTiO₂-Gd-COOH and bTiO₂-Gd-IGF1, the absorption peak of the bTiO₂-Gd-IGF1-GEM nanoprobe exhibit slightly red-shift which attributing to gemcitabine loading.

MRI and photothermal performance properties

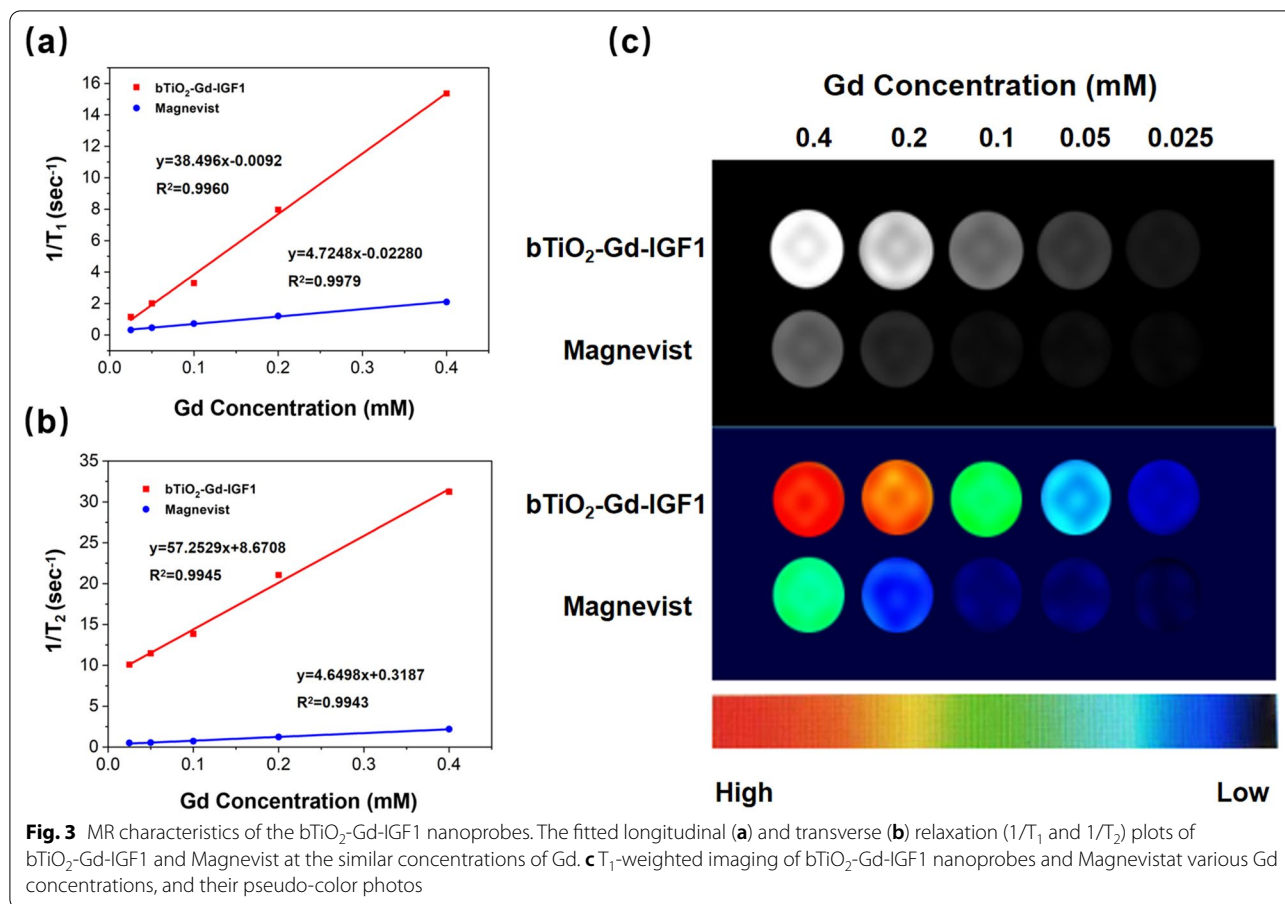
MR imaging and relaxivities of the nanoprobe were evaluated by 1.5 T MRI scanner system. Commercial contrast agent Magnevist is employed as the control. As depicted in Fig. 3a, r_1 value of bTiO₂-Gd-IGF1 is 38.496 mM⁻¹ s⁻¹, while the value of Magnevist is 4.7248 mM⁻¹ s⁻¹ at the similar concentration of Gd. It should be pointed out that the bTiO₂-Gd-IGF1 r_1 value is approximately 8.2 folds greater than the Magnevist. The markedly high bTiO₂-Gd-IGF1 r_1 value is likely

because of gadolinium coordinated by PAA with hydrophilic high molecular weight, which can enhance the rotational correlation time (τ_R) [19]. Similarly, Fig. 3b shows r_2 values of bTiO₂-Gd-IGF1 is also markedly elevated ($r_2=57.2529$ mM⁻¹ s⁻¹), compared to Magnevist ($r_2=4.6498$ mM⁻¹ s⁻¹). The bTiO₂-Gd-IGF1 r_2/r_1 ratio is approximately 1.487, which illustrates the nanoprobe are good T₁-weighted MRI contrast agent. Consequently, it is clearly indicated bTiO₂-Gd-IGF1 nanoprobe exhibit brighter T₁-weighted MRI signal than Magnevist at the same Gd concentration in Fig. 3c.

Although previous reports have proved bTiO₂ nanoprobe possess high photothermal capability [28, 29]. In this study, bTiO₂ nanoprobe were modified by PAA, PDA, as well as NH₂-PEG-COOH, therefore, photothermal performance of the prepared bTiO₂-Gd-COOH nanoprobe were evaluated. Figure 4a shows 1 mL bTiO₂-Gd-COOH dispersions (150 μg mL⁻¹) were irradiated with 808 nm laser for 10 min. With 808 nm laser increase in power, the nanoprobe temperature rises quickly after 10 min. As expected, cancer cells can undergo rapid ablation following few minutes of exposure to 50 °C [41]. When the power density of 808 nm laser was 1.2 W cm⁻², the temperature of bTiO₂-Gd-COOH dispersions were 62.2 °C after 10 min irradiation, which is considered more suitable in followed experiment. Then, bTiO₂-Gd-COOH nanoprobe underwent irradiation with 1.2 W cm⁻² of NIR laser at various concentrations of Ti from 50 to 150 μg mL⁻¹. As shown in Fig. 4b, 50 μg mL⁻¹ of bTiO₂-Gd-COOH nanoprobe reached 48.7 °C after irradiated by 808 nm laser for 10 min. In Fig. 4c, I and II are real-time photothermal images, which corresponds well with the curves of temperature in Fig. 4a, b, accordingly. In addition to photothermal performance, the photothermal stability of nanoprobe is also important. Figure 4d shows bTiO₂-Gd-COOH nanoprobe were irradiated by an 808 nm laser at 1.2 W cm⁻² for 6 cycles in 1 h. The temperature curve during heating and cooling is almost similar during in 6 cycles, which proves nanoprobe are stability during NIR irradiation.

Drug release of nanoprobe

According to the above-mentioned formula, drug loading efficiency of bTiO₂-Gd-IGF1-GEM is about 10.3%, which indicates high loading capacity of bTiO₂-Gd-IGF1 nanoprobe. Additional file 1: Fig. S1 shows the drug release curves of bTiO₂-Gd-IGF1-GEM at pH 7.4, pH 5.0, pH 5.0+NIR, respectively. The cumulative release of GEM within 27 h was 2.7 times higher in the pH 5.0 group, compared to the pH 7.4 group. The weak acid promoted drug release is probably due to the protonation of amine groups on the PDA scaffolds and/or on the GEM molecules, which partially weakens the π-π interactions



between PDA and drugs [38]. After near-infrared irradiation in pH 5.0 buffer, the total release of GEM further increased, reaching 40.8%, which is about 3.6 times than drug release at pH 7.4. NIR-responsive release pattern is mainly due to combined-photothermal effect can accelerate drug molecular motion and make GEM escape easily from the carriers [42, 43]. The above data indicate bTiO₂-Gd-IGF1-GEM nanoprobe exhibit pH and NIR co-responded drug-release properties, consequently can enhance the concentration of GEM in the tumor's weakly acidic microenvironment.

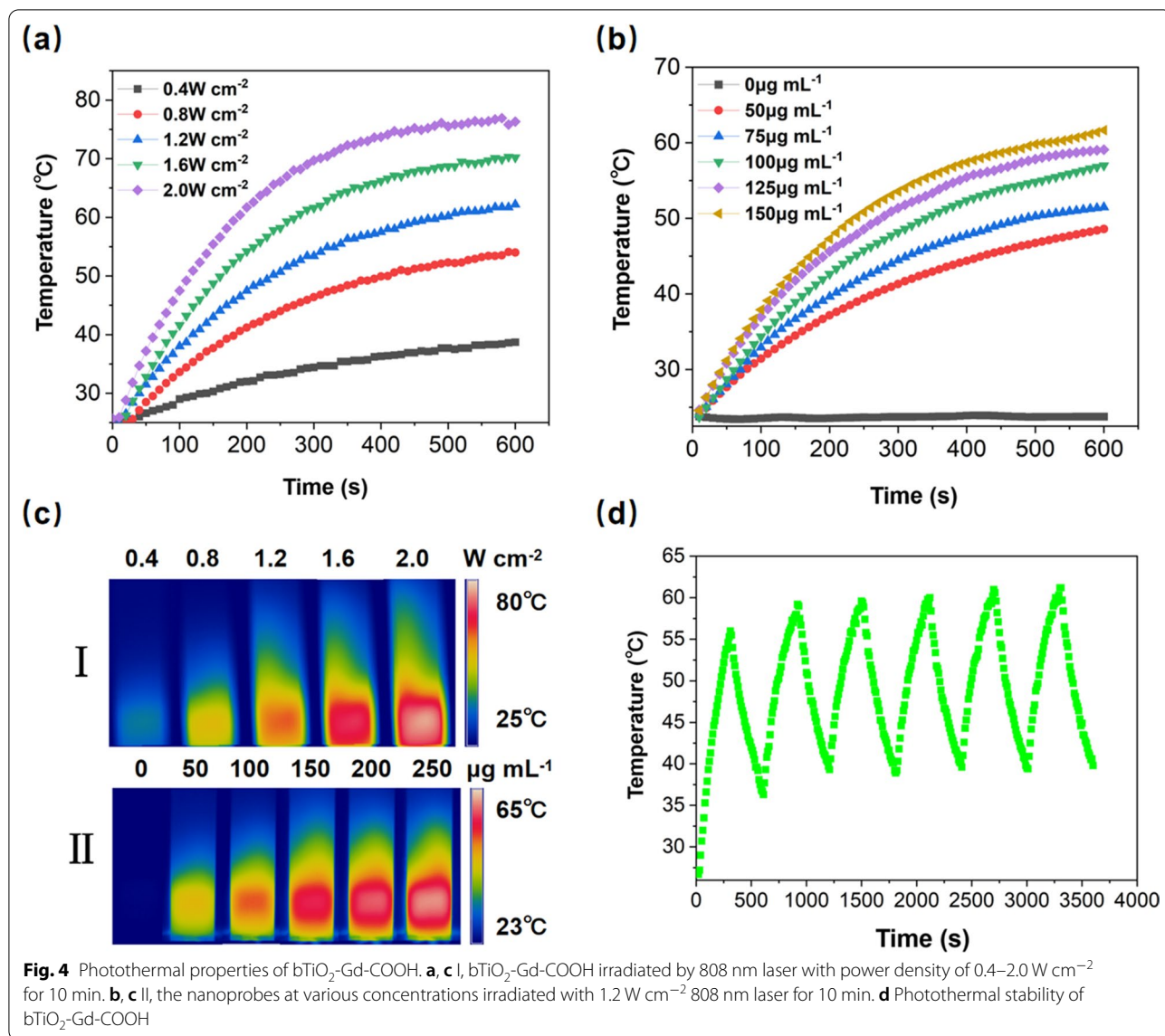
Screening of IGF1R expression in various PDAC cell lines

Western blot was employed to quantitatively determine the expression level of IGF1R in several PDAC cell lines, such as MIA PaCa-2 cells, hTERT-HPNE cells, BxPC-3 cells, and Panc-2 cells. Additional file 1: Fig. S2 shows that compared with hTERT-HPNE cells, BxPC-3 cells and Panc-2 cells, MIA PaCa-2 cells express the highest level of IGF1R. Furthermore, reports show that IGF1R express higher in drug-resistant pancreatic cells, and drug-resistance has been confirmed in MIA PaCa-2 cell line [27, 44].

Therefore, in the next experiment, we use MIA PaCa-2 cells for the cell experiment part of this experiment.

Cell uptake of nanoparticles

As described above, there are dense fibrous in pancreatic cancer. IGF1R is ubiquitously found in 40–90% of pancreatic cancer cells and stromal cells, which is ideal target sites for nanoparticles to break through the matrix and enter PDAC cells [6]. Here, in order to enhance IGF1R-target ability of nanoparticles, bTiO₂-Gd-IGF1 nanoparticles were generated via conjugation of bTiO₂-Gd-COOH with IGF1 peptides. The bTiO₂-Gd-IGF1 nanoprobe targeting ability was evaluated by XFM, ICP-OES and laser confocal microscope. By taking advantage of XFM, direct visual and quantitative localization of the titanium element was acquired. As depicted in Fig. 5a, yellow fluorescence denotes the titanium element, and red fluorescence represents biogenic element chlorine, which maps cancer cells. Weak yellow fluorescence signals were observed in the bTiO₂-Gd-COOH group, suggesting that MIA PaCa-2 cells have weak uptake of bTiO₂-Gd-COOH nanoparticles. However, intensive yellow fluorescence appears in bTiO₂-Gd-IGF1 and bTiO₂-Gd-IGF1-GEM



groups, which directly suggests that IGF1 peptide can enhance the targeting ability of nanoprobes. Followed, the target ability of nanoprobes on PDAC cells were quantitatively tested by ICP-OES. Figure 5b shows the amount of Ti element in the cells following treatment via bTiO₂-Gd-COOH or bTiO₂-Gd-IGF1 for 4 h. Similarly, the amount of Ti element of the cells in bTiO₂-Gd-IGF1 group is significantly higher than bTiO₂-Gd-COOH group, which indicates IGF1 peptide can improve the targeting ability of nanoprobes to MIA PaCa-2 cells. Finally, laser confocal microscope was employed for the observation of rhodamine 123 labeled nanoprobes uptake into MIA PaCa-2 cells. Figure 5c provides intracellular nanoprobe distribution in MIA PaCa-2 cells. Green fluorescence refers to the FITC-phalloidin

labeled cell membrane, blue fluorescence shows Hoechst 33342 nuclear staining, and red fluorescence represents rhodamine 123 labeled nanoprobe. Compared with bTiO₂-Gd-COOH group, bTiO₂-Gd-IGF1 group exhibits more aggregation in the cells, which also indicates IGF1 peptide can improve targeting capability of the nanoprobes.

Cytotoxicity assay

Previous studies have confirmed bTiO₂ nanoprobes are less toxic in vitro and in vivo [29, 30]. Here, we modified bTiO₂ with Gd, dopamine, and IGF1 peptides, so it is still critical to assess nanoprobe toxicity. Figure 6a shows the cytotoxicity of bTiO₂-Gd-COOH and bTiO₂-Gd-IGF1 on MIA PaCa-2 cells. Following 24 h's

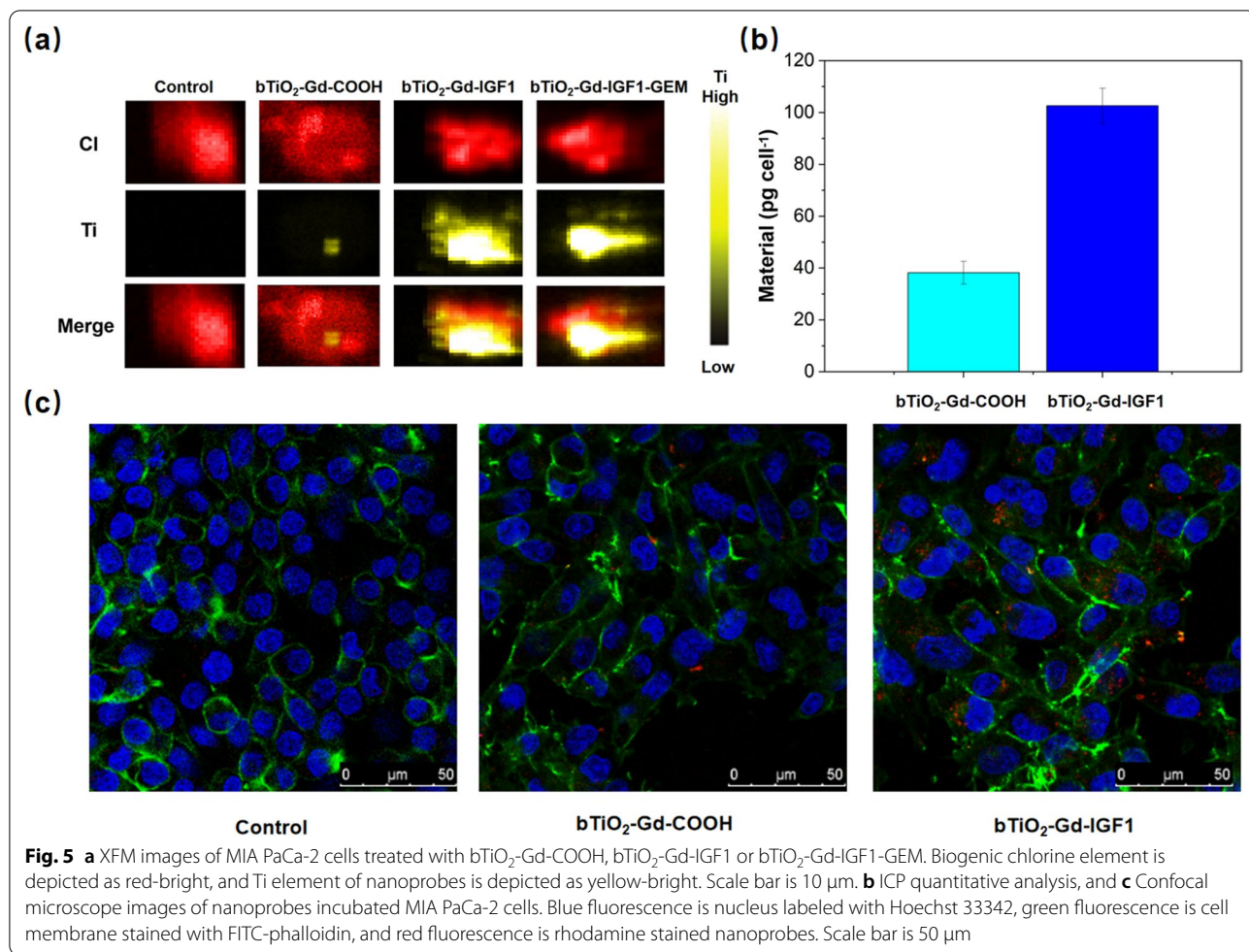


Fig. 5 **a** XFM images of MIA PaCa-2 cells treated with bTiO₂-Gd-COOH, bTiO₂-Gd-IGF1 or bTiO₂-Gd-IGF1-GEM. Biogenic chlorine element is depicted as red-bright, and Ti element of nanoprobes is depicted as yellow-bright. Scale bar is 10 μm. **b** ICP quantitative analysis, and **c** Confocal microscope images of nanoprobes incubated MIA PaCa-2 cells. Blue fluorescence is nucleus labeled with Hoechst 33342, green fluorescence is cell membrane stained with FITC-phalloidin, and red fluorescence is rhodamine stained nanoprobes. Scale bar is 50 μm

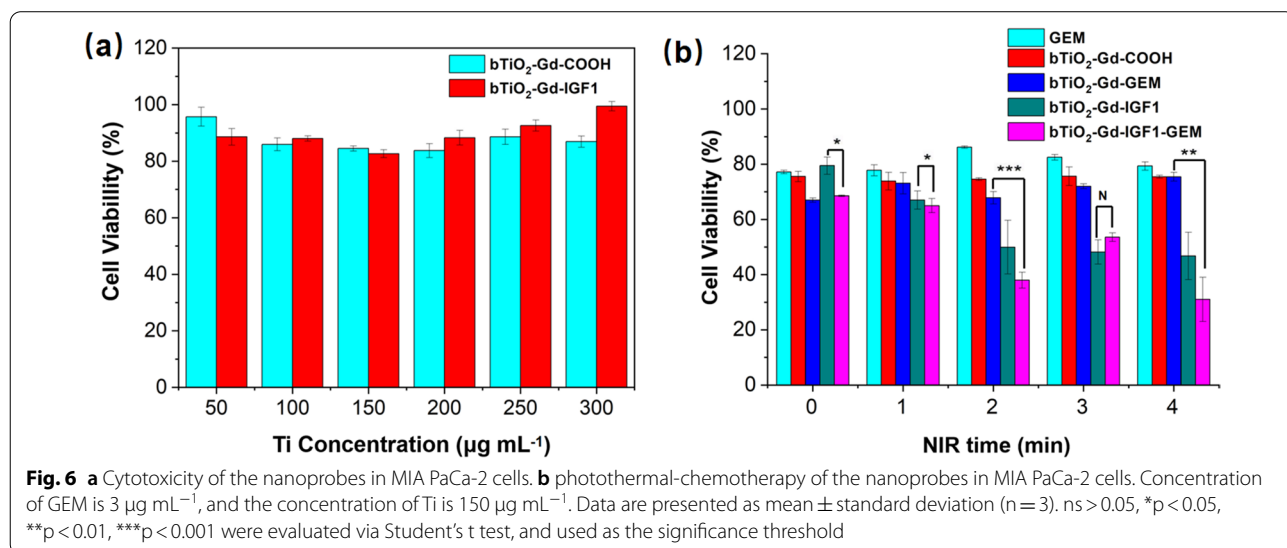


Fig. 6 **a** Cytotoxicity of the nanoprobes in MIA PaCa-2 cells. **b** photothermal-chemotherapy of the nanoprobes in MIA PaCa-2 cells. Concentration of GEM is 3 μg mL⁻¹, and the concentration of Ti is 150 μg mL⁻¹. Data are presented as mean ± standard deviation (n = 3). ns > 0.05, *p < 0.05, **p < 0.01, ***p < 0.001 were evaluated via Student's t test, and used as the significance threshold

incubation, the cell viability is higher than 80% in the nanoprobe's concentration range of 50–300 $\mu\text{g mL}^{-1}$, which confirms the nanoprobe are low cytotoxicity. The cell survival rate of bTiO₂-Gd-IGF1 incubated cells seem to increase when Ti concentration is over 200 $\mu\text{g mL}^{-1}$. This may be attributed to more nanoprobe entered the cells and the cell color deepened, which affected the absorptions.

PTT and chemotherapy of pancreatic cancer in vitro

Figure 6b shows PTT and chemotherapy of nanoprobe in PDAC cells. MIA PaCa-2 cells were maintained in DMEM, GEM, bTiO₂-Gd-COOH, bTiO₂-Gd-GEM, and bTiO₂-Gd-IGF1 or bTiO₂-Gd-IGF1-GEM for 2 h. When there is no laser irradiation, cell viabilities are $77.2 \pm 0.6\%$ (GEM), $75.5 \pm 1.9\%$ (bTiO₂-Gd-COOH), $67.0 \pm 0.8\%$ (bTiO₂-Gd-GEM), $79.5 \pm 3.1\%$ (bTiO₂-Gd-IGF1) and $68.6 \pm 0.3\%$ (bTiO₂-Gd-IGF1-GEM), respectively. The results show that only 22.8% of the cells can be killed by GEM after 2 h of incubation, which indicates drug-resistance of the cells. Cell survival rate in bTiO₂-Gd-GEM and bTiO₂-Gd-IGF1-GEM group is significantly lower than that in bTiO₂-Gd-COOH and bTiO₂-Gd-IGF1 group, which may be due to the killing effect of GEM. After NIR laser irradiation for 4 min, cell viabilities are $79.4 \pm 1.5\%$ (GEM), $75.4 \pm 0.5\%$ (bTiO₂-Gd-COOH), $75.4 \pm 1.6\%$ (bTiO₂-Gd-GEM), $46.8 \pm 8.6\%$ (bTiO₂-Gd-IGF1) and $31.0 \pm 8.6\%$ (bTiO₂-Gd-IGF1-GEM), respectively. Relative to PTT or chemotherapy alone, killing efficiency in photothermal-chemotherapy group is more significant. In particular, cell killing rate in bTiO₂-Gd-IGF1-GEM group can reach 69%.

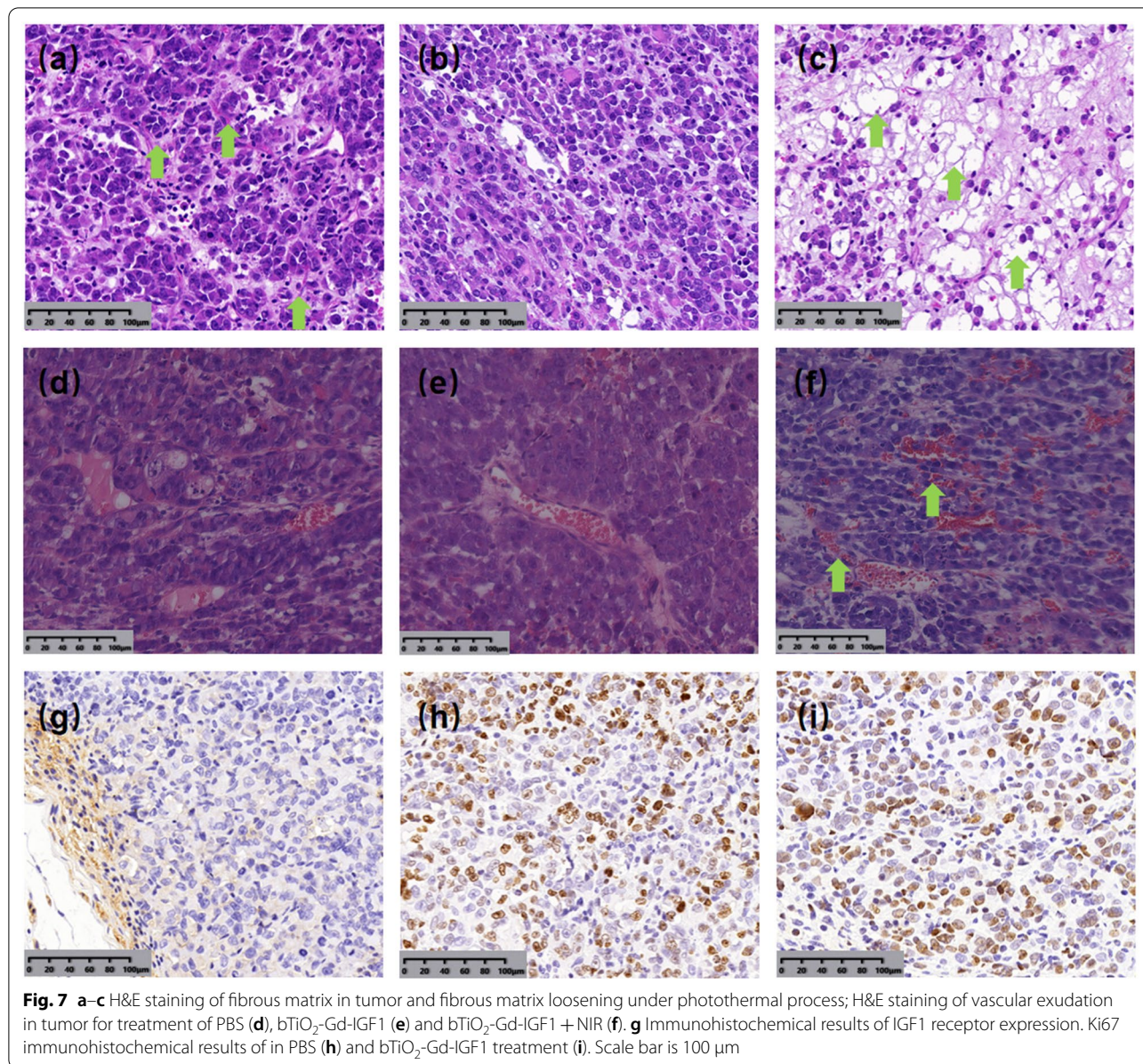
The in vitro photothermal-chemotherapy performance is also visually examined using live/dead cell staining via calcein AM/PI reagents. According to Additional file 1: Fig. S3, red fluorescence (PI) marks dead cells, and green fluorescence (Calcein-AM) stains live cells. Most MIA PaCa-2 cells can survive under 1.2 W cm⁻² of 808 nm NIR irradiation alone, indicating 808 nm NIR irradiation at 1.2 W cm⁻² is safety to cells. However, MIA PaCa-2 cells are killed in varying degrees when the cells were maintained in the same concentrations of GEM, bTiO₂-Gd-COOH, bTiO₂-Gd-GEM, bTiO₂-Gd-IGF1, bTiO₂-Gd-IGF1-GEM, and irradiated by 1.2 W cm⁻² of 808 nm NIR, while bTiO₂-Gd-IGF1-GEM nanoprobe induce more extensive cell death. The live/dead cell staining results are consistent with the MTT results, further indicating that the photothermal-chemotherapy has a more significant killing effect, and can overcome drug-resistance of MIA PaCa-2 PDAC cells.

Photothermal imaging, MRI, and synergetic photothermal-chemotherapy in vivo

The in vivo toxicity assessment of the nanoprobe is carried out by injecting PBS, bTiO₂-Gd-COOH, bTiO₂-Gd-IGF1 into balb/c mice through tail vein. Additional file 1: Fig. S4a shows the weight change of mice within 1 month after nanoprobe injection. Additional file 1: Fig. S4b, c are blood routine index and the histological analysis of the organs after injection for 1 month. Relative to PBS controls, we observed no marked changes in body weight and blood routine indexes, meanwhile no damage in tissues or other lesions like pulmonary fibrosis, inflammatory, or necrosis are evident in bTiO₂-Gd-COOH and bTiO₂-Gd-IGF1 administered groups. The above results indicate that the prepared nanoprobe offer no toxicity to mice at the doses used for 1 month.

After the mouse pancreatic cancer tumor model was constructed, HE staining was performed on tumor tissue. In Fig. 7a, the arrows show that tumor contained a large amount of stroma cells, which suggests the tumor model is successfully constructed. In order to detect the matrix barrier loosening and vascular permeability improving in photothermal process, bTiO₂-Gd-IGF1 nanoprobe were injected into the tumor site, and then underwent irradiation with or without 808 nm NIR laser. It can be seen from Fig. 7b–f, compared with unirradiated control group (Fig. 7a), the tumor matrix is loosened, the vascular permeability is increased, and the red blood cells extravasate into the surrounding tissue after near-infrared irradiation. Immunohistochemical analysis (Fig. 7g) shows that IGF1R is ubiquitously found in both of tumor cells and fibrous stromal cells, which is consistent with literature reports [6, 27]. Subsequently, we examined the impact of bTiO₂-Gd-IGF1 on the proliferation of PDAC tumor cells in vivo. Studies have found that IGF1 polypeptide can promote tumor cell proliferation, while Zhou et al. demonstrated IGF1 modified iron oxide nanoparticles could reduce IGF1's growth-stimulating function, but retain the targeting ability [6]. To further confirm this phenomenon, we injected the tumor with PBS or bTiO₂-Gd-IGF1 twice, and then analyzed with Ki67 immunohistochemistry. As depicted in Fig. 7h, i, relative to PBS controls, repeatedly injected tumor with bTiO₂-Gd-IGF1 does not enhance cell proliferation index. Therefore, modified bTiO₂-Gd-COOH with IGF1 could decrease IGF1's growth-stimulating activity but still retain targeting ability. Nevertheless, its underlying mechanism is still undetermined.

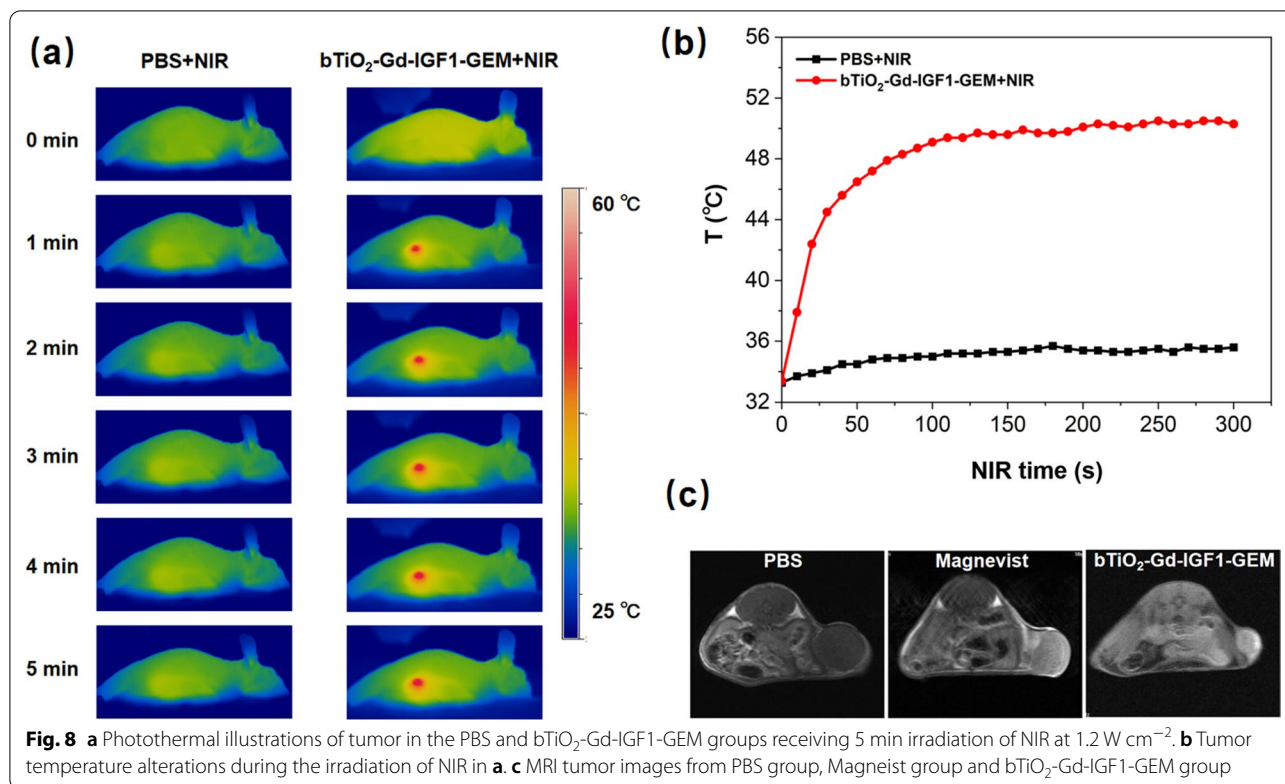
Followed, photothermal images of tumors are analyzed in PBS group and bTiO₂-Gd-IGF1-GEM group under NIR irradiation. As depicted in Fig. 8a, relative to controls,



tumoral temperature rapidly increase in NIR irradiated bTiO₂-Gd-IGF1-GEM group. In Fig. 8b, the tumoral temperature in PBS group increases from 33.3 to 35.6 °C after NIR irradiation, indicating that NIR is safety. While tumoral temperature in the bTiO₂-Gd-IGF1-GEM group rises from 33.4 to 50.3 °C after NIR irradiation, cancer cells can be rapidly eliminated after only a few minutes of exposure. Hence, the bTiO₂-Gd-IGF1-GEM group after NIR irradiation can easily kill cancer cells according to previous study suggested expose of cells in 50 °C [41]. Figure 8c shows MRI images in various groups. As shown in the picture, the intratumoral T₁-weighted MR imaging of PBS is poor, while bTiO₂-Gd-IGF1-GEM nanoprobe is

better than that of Magnevist at the same Gd concentration, which confirms the feasibility MRI performance of bTiO₂-Gd-IGF1-GEM nanoprobes.

To evaluate in vivo synergetic photothermal-chemotherapy, the tumor-injected animals were arbitrarily separated into six classes. The PBS + NIR group was PBS administered, followed by irradiation with NIR laser. The GEM group was administered with GEM. The bTiO₂-Gd-IGF1 + NIR group was bTiO₂-Gd-IGF1 administered, followed by irradiation with NIR. Likewise, the bTiO₂-Gd-IGF1-GEM or bTiO₂-Gd-IGF1-GEM + NIR group was bTiO₂-Gd-IGF1-GEM administered, followed by

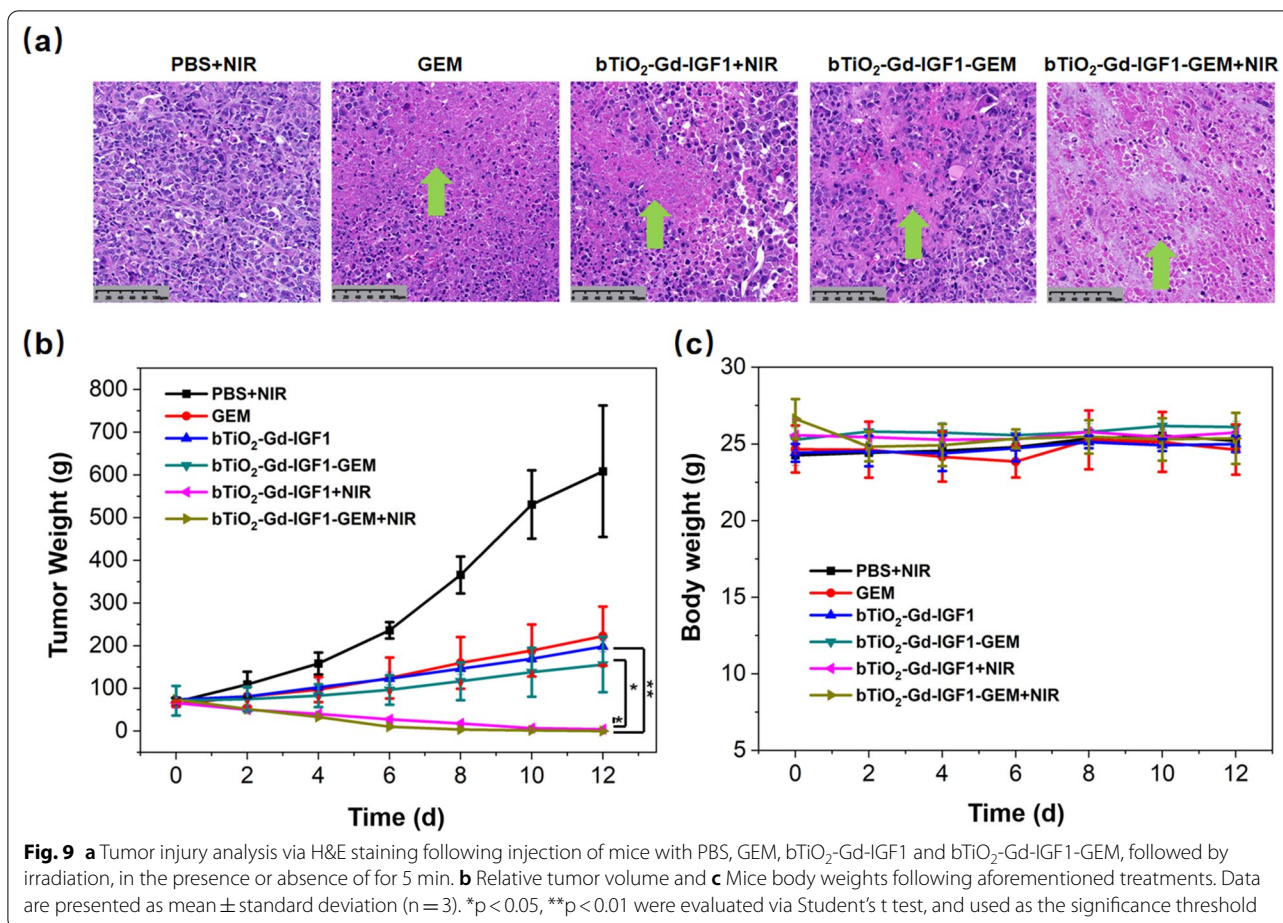


irradiation without or with NIR, respectively. In order to prove that cooperative photothermal-chemotherapy can loosen matrix barrier and overcome drug-resistance, part of mice were euthanized shortly following the irradiation of NIR, and tumors were assessed via H&E staining. According to Fig. 9a, no marked pathological damage was observed in the PBS + NIR group. There are different degrees of cell damage in the GEM, bTiO₂-Gd-IGF1 and bTiO₂-Gd-IGF1-GEM groups, the green arrows in the figure represent necrosis of tumor tissue. In the bTiO₂-Gd-IGF1-GEM + NIR group, most of the cancer cells are eliminate, indicating that advantages of synergetic therapy. Figure 9b provides the changes of tumor volume after treatments, based on the treatments in Fig. 9a. Following 12 days, the tumor sizes are 609.0 ± 153.7, 222.5 ± 69.3, 198.2 ± 12.6, 156.0 ± 64.9, 4.1 ± 1.3 and 0.3 ± 0.4 mm³ in the PBS + NIR, GEM, bTiO₂-Gd-IGF1, bTiO₂-Gd-IGF1-GEM, bTiO₂-Gd-IGF1 + NIR and bTiO₂-Gd-IGF1-GEM + NIR groups, respectively. Relative to the bTiO₂-Gd-IGF1 + NIR or bTiO₂-Gd-IGF1-GEM group, the tumors in bTiO₂-Gd-IGF1-GEM + NIR group significantly reduce, which indicate synergetic photothermal-chemotherapy not only can loosen matrix barrier, but also can overcome drug-resistance. The toxic effects of the treatments were evaluated by measuring body weight

of the mice within 12 days. In Fig. 9c, body weights of mice in each group did not change significantly, which proves that the treatments are safety and tolerable in pancreatic tumor models.

Conclusions

In summary, to break matrix barrier and reverse drug resistance in PDAC, this study proposes a dual-targeted photothermal-chemotherapy strategy in PDAC cells and stromal cells, and prepare bTiO₂-Gd-GEM-IGF1 nanoprobes. First, WB and pathology results confirm IGF1R is ubiquitously found in MIA PaCa-2 cells and their tumor model, meanwhile MIA PaCa-2 cells are resistant to gemcitabine. The IGF1 modified nanoprobes exhibit stronger targeting ability to MIA PaCa-2 cells. Next, cell experiments show that the killing effect of synergistic treatment on MIA PaCa-2-resistant cells is about 3.3 times than chemotherapy alone, which suggest reversal of drug-resistance. Followed, histological experiments prove photothermal can loosen the fibrous matrix of pancreatic cancer model and increase the permeability of blood vessels. Therefore, in vivo results show that tumor models are almost completely cured after 12 days of combined treatments. In conclusion, we provide a more effective approach for treating pancreatic cancer through matrix barrier loosening and drug resistance reverse, and also



provide an experimental basis for applying black TiO₂ in synergistic photothermal-chemotherapy in pancreatic cancer.

Supplementary Information

The online version contains supplementary material available at <https://doi.org/10.1186/s12951-022-01525-3>.

Additional file 1: Figure S1. PH and NIR co-responded drug-release of bTiO₂-Gd-IGF1-GEM. **Figure S2.** The IGF1R expression in MIA PaCa-2 cells, hTERT-HPNE cells, BxPC-3 cells, and Panc-2 cells. **Figure S3.** Live/dead cell staining following various treatments. Green and red fluorescence denote live and dead cells, respectively. Scale bar is 20 μm. **Figure S4.** In vivo toxicity analysis of nanoprobe on balb/c mice. The changes of (a) body weight, (b) routine blood indexes, and (c) organ histological analysis after injected with PBS, bTiO₂-Gd-COOH, bTiO₂-Gd-IGF1 for 1 month. Scale bar is 100 μm.

Acknowledgements

The authors thank National Synchrotron Radiation Laboratory in Hefei for soft X-ray imaging and Shanghai Synchrotron Radiation Facility at Line BL15U for X-ray fluorescence imaging.

Author contributions

KX, LJ and LX did most of the in vitro and in vivo experiments. KX prepared figures and wrote the manuscript. YZ and LH did part of animal experiments. CP

and YL analyzed the results of MRI. JY and RZ analyzed the results of spectra. WT analyzed the figures of tissue staining. JW, AW and WR provided financial support, supervised the study, and reviewed the manuscript. All authors read and approved the final manuscript.

Funding

This work was supported by the National Natural Science Foundation of China (82172004, 32025021, 31971292, 32171359), Scientific Research Foundation of the National Health Commission—Major Science and Technology Project of Medicine and Health of Zhejiang Province (WKJ-ZJ-1912), Natural Science Foundation of Zhejiang Province (Y20H180008), the Zhejiang Province Financial Supporting (2020C03110, LGF19C100001), the Key Scientific and Technological Special Project of Ningbo City (2020Z094), Ningbo Public Welfare Science and Technology Project (2021JCGY020358), the Science & Technology Bureau of Ningbo City (202003N4001, 2021J254), and the Users with Excellence Program of Hefei Science Center, CAS (2020HSC-UE006).

Availability of data and materials

All the data generated or analyzed during this study are included in the article.

Declarations

Ethics approval and consent to participate

For animal experiments, animal care and handling procedures were in agreement with the guidelines of the Regional Ethics Committee for Animal Experiments at Ningbo University (Permit No. SYXK Zhe 2019-0005).

Consent for publication

All of authors agreed to submit this manuscript.

Competing interests

The authors declare that there are no competing interests.

Author details

¹Department of Radiology, the Affiliated Hospital of Medical School, Ningbo University, 247 Renmin Road, Jiangbei District, Ningbo 315020, Zhejiang, China. ²Cixi Institute of Biomedical Engineering, International Cooperation Base of Biomedical Materials Technology and Application, Chinese Academy of Science (CAS) Key Laboratory of Magnetic Materials and Devices & Zhejiang Engineering Research Center for Biomedical Materials, Ningbo Institute of Materials Technology and Engineering, CAS, 1219 ZhongGuan West Road, Ningbo 315201, China. ³Advanced Energy Science and Technology Guangdong Laboratory, Huizhou 516000, China. ⁴Key Laboratory of Diagnosis and Treatment of Digestive System Tumors of Zhejiang Province, Ningbo 315016, China.

Received: 14 May 2022 Accepted: 23 June 2022

Published online: 06 July 2022

References

- Rahib L, Smith BD, Aizenberg R, Rosenzweig AB, Fleshman JM, Matrisian LM. Projecting cancer incidence and deaths to 2030: the unexpected burden of thyroid, liver, and pancreas cancers in the United States. *Cancer Res.* 2014;74:2913–21.
- Rawla P, Sunkara T, Gaduputi V. Epidemiology of pancreatic cancer: global trends, etiology and risk factors. *World J Oncol.* 2019;10:10–27.
- Siegel RL, Miller KD, Jemal A. Cancer statistics, 2018. *CA Cancer J Clin.* 2018;68:7–30.
- Amrutkar M, Gladhaug IP. Pancreatic cancer chemoresistance to gemcitabine. *Cancers (Basel).* 2017;9:157.
- Adamska A, Domenichini A, Falasca M. Pancreatic Ductal Adenocarcinoma: current and evolving therapies. *Int J Mol Sci.* 2017;18:1338.
- Zhou H, Qian W, Uckun FM, Wang L, Wang YA, Chen H, Kooby D, Yu Q, Lipowska M, Staley CA, Mao H, Yang L. IGF1 receptor targeted theranostic nanoparticles for targeted and image-guided therapy of pancreatic cancer. *ACS Nano.* 2015;9:7976–91.
- Sarvepalli D, Rashid MU, Rahman AU, Ullah H, Hussain I, Hasan B, Jehanzeb S, Khan AK, Jain AG, Khetpal N, Ahmad S. Gemcitabine: a review of chemo-resistance in pancreatic cancer. *Crit Rev Oncog.* 2019;24:199–212.
- Yoneura N, Takano S, Yoshitomi H, Nakata Y, Shimazaki R, Kagawa S, Furukawa K, Takayashiki T, Kuboki S, Miyazaki M, Ohtsuka M. Expression of annexinII and stromal tenascinC promotes epithelial to mesenchymal transition and correlates with distant metastasis in pancreatic cancer. *Int J Mol Med.* 2018;42:821–30.
- Zheng P, Ding J. Calcium ion nanomodulators for mitochondria-targeted multimodal cancer therapy. *Asian J Pharm Sci.* 2022;17:3.
- Jiang Z, Liu Y, Shi R, Feng X, Xu W, Zhuang X, Ding J, Chen X. Versatile polymer-initiating biomineralization for tumor blockade therapy. *Adv Mater.* 2022;34: e2110094.
- Zheng P, Ding B, Shi R, Jiang Z, Xu W, Li G, Ding J, Chen X. A multichannel Ca²⁺ nanomodulator for multilevel mitochondrial destruction-mediated cancer therapy. *Adv Mater.* 2021;33: e2007426.
- Chen J, Jiang Z, Zhang Y, Ding J, Chen X. Smart transformable nanoparticles for enhanced tumor theranostics. *Appl Phys Rev.* 2021;8: 041321.
- Zheng C, Li M, Ding J. Challenges and opportunities of nanomedicines in clinical translation. *Bio Integration.* 2021;2:57–60.
- Yu S, Zhou Y, Sun Y, Wu S, Xu T, Chang YC, Bi S, Jiang LP, Zhu JJ. Endogenous mRNA triggered DNA-Au nanomachine for in situ imaging and targeted multimodal synergistic cancer therapy. *Angew Chem Int Ed Engl.* 2021;60:5948–58.
- Li Y, Yue S, Cao J, Zhu C, Wang Y, Hai X, Song W, Bi S. pH-responsive DNA nanomicelles for chemo-gene synergetic therapy of anaplastic large cell lymphoma. *Theranostics.* 2020;10:8250–63.
- Vennin C, Méléneć P, Rouet R, Nobis M, Cazet AS, Murphy KJ, Herrmann D, Reed DA, Lucas MC, Warren SC, Elgundi Z, Pinese M, Kalna G, Rode D, Samuel M, Zaratzian A, Grey ST, Da Silva A, Leung W, Australian Pancreatic Genome Initiative (APGI), Mathivanan S, Wang Y, Braithwaite AW, Christ D, Benda A, Parkin A, Phillips PA, Whitelock JM, Gill AJ, Sansom OJ, Croucher DR, Parker BL, Pajic M, Morton JP, Cox TR, Timpson P. CAF hierarchy driven by pancreatic cancer cell p53-status creates a pro-metastatic and chemoresistant environment via perlecan. *Nat Commun.* 2019;10:3637.
- Qu C, Wang Q, Meng Z, Wang P. Cancer-associated fibroblasts in pancreatic cancer: should they be deleted or reeducated? *Integr Cancer Ther.* 2018;17:1016–9.
- Teng T, Lin R, Lin Z, Ke K, Lin X, Pan M, Zhang D, Huang H. Photo-thermal augment stromal disrupting effects for enhanced abraxane synergy chemotherapy in pancreatic cancer PDX mode. *Biomater Sci.* 2020;8:3278–85.
- Tang SC, Chen YC. Novel therapeutic targets for pancreatic cancer. *World J Gastroenterol.* 2014;20:10825–44.
- Minami K, Shinsato Y, Yamamoto M, Takahashi H, Zhang S, Nishizawa Y, Tabata S, Ikeda R, Kawahara K, Tsujikawa K, Chijiwa K, Yamada K, Akiyama S, Pérez-Torras S, Pastor-Anglada M, Furukawa T, Yasuo T. Ribonucleotide reductase is an effective target to overcome gemcitabine resistance in gemcitabine-resistant pancreatic cancer cells with dual resistant factors. *J Pharmacol Sci.* 2015;127:319–25.
- Zhang D, Li L, Jiang H, Li Q, Wang-Gillam A, Yu J, Head R, Liu J, Ruzinova MB, Lim KH. Tumor-stroma IL-1 β -IRAK4 feedforward circuitry drives tumor fibrosis, chemoresistance, and poor prognosis in pancreatic cancer. *Cancer Res.* 2018;78:1700–12.
- Tian G, Zhang X, Zheng X, Yin W, Ruan L, Liu X, Zhou L, Yan L, Li S, Gu Z, Zhao Y. Multifunctional Rbx WO₃ nanorods for simultaneous combined chemo-photothermal therapy and photoacoustic/CT imaging. *Small.* 2015;10:4160–70.
- Xie M, Yang M, Sun X, Yang N, Deng T, Li Y, Shen H. WS₂ nanosheets functionalized by biomimetic lipids with enhanced dispersibility for photothermal and chemo combination therapy. *J Mater Chem B.* 2020;8:2331–42.
- Poudel BK, Gupta B, Ramasamy T, Thapa RK, Pathak S, Oh KT, Jeong JH, Choi HG, Yong CS, Kim JO. PEGylated thermosensitive lipid-coated hollow gold nanoshells for effective combinational chemo-photothermal therapy of pancreatic cancer. *Colloids Surf B Biointerfaces.* 2017;160:73–83.
- Khan M, Boumati S, Arib C, Thierno Diallo A, Djaker N, Doan BT, Spadavecchia J. Doxorubicin (DOX) gadolinium-gold-complex: a new way to tune hybrid nanorods as theranostic agent. *Int J Nanomed.* 2021;16:2219–36.
- Zhao R, Han X, Li Y, Wang H, Ji T, Zhao Y, Nie G. Photothermal effect enhanced cascade-targeting strategy for improved pancreatic cancer therapy by gold nanoshell@mesoporous silica nanorod. *ACS Nano.* 2017;11:8103–13.
- Ireland L, Santos A, Ahmed MS, Rainer C, Nielsen SR, Quaranta V, Weyher-Czernilofsky U, Engle DD, Perez-Mancera PA, Coupland SE, Taktak A, Bogenrieder T, Tuveson DA, Campbell F, Schmid MC, Mielgo A. Chemoresistance in pancreatic cancer is driven by Stroma-derived insulin-like growth factors. *Cancer Res.* 2016;76:6851–63.
- Ren W, Yan Y, Zeng L, Shi Z, Gong A, Schaaf P, Wang D, Zhao J, Zou B, Yu H, Chen G, Brown EM, Wu A. A near infrared light triggered hydrogenated black TiO₂ for cancer photothermal therapy. *Adv Healthc Mater.* 2015;4:1526–36.
- Ren W, Iqbal MZ, Zeng L, Chen T, Pan Y, Zhao J, Yin H, Zhang L, Zhang J, Li A, Wu A. Black TiO₂ based core-shell nanocomposites as doxorubicin carriers for thermal imaging guided synergistic therapy of breast cancer. *Nanoscale.* 2017;9:11195–204.
- Wang S, Ren W, Wang J, Jiang Z, Saeed M, Zhang L, Li A, Wu A. Black TiO₂ based nanoprobes for T₁-weighted MRI guided photothermal therapy in CD133 high expressed pancreatic cancer stem-like cells. *Biomater Sci.* 2018;6:2209–18.
- Han X, Huang J, Jing X, Yang D, Lin H, Wang Z, Li P, Chen Y. Oxygen-deficient black titania for synergistic/enhanced sonodynamic and photoinduced cancer therapy at near infrared-II biowindow. *ACS Nano.* 2018;12:4545–55.
- Tao N, Li H, Deng L, Zhao S, Ouyang J, Wen M, Chen W, Zeng K, Wei C, Liu YN. A cascade nanozyme with amplified sonodynamic therapeutic effects through comodulation of hypoxia and immunosuppression against cancer. *ACS Nano.* 2021;16(1):485–501.
- Saeed M, Iqbal MZ, Ren W, Xia Y, Khan WS, Wu A. Tunable fabrication of new theranostic Fe₃O₄-black TiO₂ nanocomposites: dual wavelength

- stimulated synergistic imaging-guided phototherapy in cancer. *J Mater Chem B*. 2019;7:210–23.
34. Ren W, Zeng L, Shen Z, Xiang L, Gong A, Zhang J, Mao C, Li A, Paunesku T, Woloschak GE. Enhanced doxorubicin transport to multidrug resistant breast cancer cells via TiO₂ nanocarriers. *RSC Adv*. 2013;3:20855–61.
 35. Du Y, Ren W, Li Y, Zhang Q, Zeng L, Chi C, Wu A, Tian J. The enhanced chemotherapeutic effects of doxorubicin loaded PEG coated TiO₂ nanocarriers in an orthotopic breast tumor bearing mouse model. *J Mater Chem B*. 2015;3:1518–28.
 36. Hauser D, Septiadi D, Turner J, Petri-Fink A, Rothen-Rutishauser B. From bioinspired glue to medicine: polydopamine as a biomedical material. *Materials (Basel)*. 2020;13:1730.
 37. Zhu Z, Su M. Polydopamine nanoparticles for combined chemo- and photothermal cancer therapy. *Nanomaterials (Basel)*. 2017;7:160.
 38. Wang X, Zhang J, Wang Y, Wang C, Xiao J, Zhang Q, Cheng Y. Multi-responsive photothermal-chemotherapy with drug-loaded melanin-like nanoparticles for synergetic tumor ablation. *Biomaterials*. 2015;81:114–24.
 39. Guan S, Liu X, Zhang Y, Liu Y, Wang L, Liu Y. Synthesis and characterization of polycaprolactone modified trimellitate nano-lubricant. *Materials (Basel)*. 2019;12:2273.
 40. Maity M, Das S, Maiti NC. Stability and binding interaction of bilirubin on a gold nano-surface: steady state fluorescence and FT-IR investigation. *Phys Chem Chem Phys*. 2014;16:20013–24.
 41. Wang X, Cheng L. Multifunctional two-dimensional nanocomposites for photothermal-based combined cancer therapy. *Nanoscale*. 2019;11:15685–708.
 42. Qi Z, Shi J, Zhang Z, Cao Y, Li J, Cao S. PEGylated graphene oxide-capped gold nanorods/silica nanoparticles as multifunctional drug delivery platform with enhanced near-infrared responsiveness. *Mater Sci Eng C Mater Biol Appl*. 2019;104: 109889.
 43. Qiu Y, Ding D, Sun W, Feng Y, Huang D, Li S, Meng S, Zhao Q, Xue LJ, Chen H. Hollow mesoporous carbon nanospheres for imaging-guided light-activated synergistic thermo-chemotherapy. *Nanoscale*. 2019;11:16351–61.
 44. Cao J, Yang J, Ramachandran V, Arumugam T, Deng D, Li Z, Xu L, Logsdon CD. TM4SF1 promotes gemcitabine resistance of pancreatic cancer in vitro and in vivo. *PLoS ONE*. 2015;10: e0144969.

Publisher's Note

Springer Nature remains neutral with regard to jurisdictional claims in published maps and institutional affiliations.

Ready to submit your research? Choose BMC and benefit from:

- fast, convenient online submission
- thorough peer review by experienced researchers in your field
- rapid publication on acceptance
- support for research data, including large and complex data types
- gold Open Access which fosters wider collaboration and increased citations
- maximum visibility for your research: over 100M website views per year

At BMC, research is always in progress.

Learn more biomedcentral.com/submissions

